J Comput Electron (2010) 9: 206–210
DOI 10.1007/s10825-010-0341-8

Self-consistent Poisson-Schrödinger-Monte Carlo solver: electron mobility in silicon nanowires

E.B. Ramayya · I. Knezevic

Published online: 28 October 2010

Abstract Silicon nanowires (SiNWs) are quasi-one-dimensional structures in which electrons are spatially confined in two directions and are free to move in one direction. They are ideal test structures for investigating the effect of two-dimensional (2D) electron confinement. A self-consistent 2D Poisson-2D Schrödinger solver coupled with a Monte-Carlo transport kernel can accurately model the electronic transport in long SiNWs. In this paper we provide a detailed description of the coupled Poisson-Schrödinger-Monte Carlo solver as employed to compute the electron mobility in SiNWs.

Keywords Nanowires · Monte Carlo · Low-field mobility · Electron mobility · Self-consistent Schrödinger-Poisson solver

1 Introduction

The theoretical study of electronic transport in semiconductor nanowires started with the seminal work of Sakaki [1] in 1980. Sakaki showed that the elastic scattering in nanowires (NWs) is drastically suppressed due to a reduction in the final density of states (DOS) for scattering. Electrons in NWs are confined in two transverse directions and are free to move only along the axis of the wire. At room temperature, transport within each subband and transitions among subbands can essentially be described semiclassically, using the Boltzmann transport equation (BTE). Initial theoretical work on electron transport in SiNWs relied on the relaxation time approximation for the BTE and an infinite potential for the confinement in the transverse directions. In the regime where transport is dominated by scattering, an accurate description of transport can be obtained by using a Monte Carlo solver for the BTE [2] combined with the two-dimensional (2D) Poisson and Schrödinger equation solvers for the description of charge and the confining potential [3]. This is the state-of-the-art approach to calculate the diffusive-regime low-field electron mobility which is one of the most important parameters that determines the performance of field-effect transistors (FETs), thermoelectric (TE) coolers, and sensors. It has been shown that the effective mass approach remains accurate down to 3 nm wire thickness [4], while for ultrathin wires the use of atomistic approaches becomes important [4–9].

Experimental and theoretical results of electron mobility in SiNWs have until recently been inconclusive: the works of Sakaki [1], Cui et al. [10], Koo et al. [11], and Sharma et al. [12] show higher mobility in SiNWs compared to bulk MOSFETs, whereas Kotlyar et al. [13], Jin et al. [14], and more recently other research groups [15–17] have shown that the mobility in a SiNW decreases with cross section. Recent measurements by Gunawan et al. [18] from which parasitics have been carefully eliminated, show a drop in the electron mobility with respect to bulk MOSFETs. The contradiction stems from two opposing effects that determine the electron mobility as we move from 2D to 1D structures: one is a decrease in the density of states (DOS) for scattering [1] that results in reduced scattering rates and thereby an enhancement in the mobility; the second is an increase in the so-called electron-phonon wavefunction overlap [13] that results in increased electron-phonon scattering rates and

E.B. Ramayya (✉) · I. Knezevic
Department of Electrical and Computer Engineering,
University of Wisconsin–Madison, Madison, WI 53706, USA
e-mail: ramayya@wisc.edu

I. Knezevic
e-mail: knezevic@engr.wisc.edu

consequently lower mobility. While important, these two competing phenomena do not paint a full picture of low-field transport in SiNWs, in which the effect of spatial confinement on the scattering due to surface roughness and acoustic phonons must be addressed.

In this work, we compute the electron mobility in gated SiNWs with square cross section by accounting for the scattering of electrons due to confined acoustic phonons, intervalley phonons, and imperfections at the Si-SiO_2 interface. The simulator developed to calculate the electron mobility has two components: the first is a self-consistent 2D Poisson-2D Schrödinger solver and the second is a Monte-Carlo transport kernel. The former is used to calculate the electronic states and the self-consistent potential distribution along the cross section of the wire and the latter simulates the transport along the wire axis. The finite barrier at the Si-SiO_2 interface results in the electron wavefunction penetration through the interface and into the oxide. The wavefunction penetration is accounted for by including a few mesh points in the oxide while solving the Schrödinger equation. ARPACK package [19] was used to solve the 2D Schrödinger equation and successive over-relaxation (SOR) method was used to solve the 2D Poisson equation.

2 Mobility calculation and simulator components

2.1 Device structure

The SiNW considered in this study is the channel of the ultra-thin, ultra-narrow SOI MOSFET that was originally proposed by Majima et al. [20]. The thickness of the gate oxide, buried oxide, and the silicon handle layer are 25 nm, 80 nm, and 700 nm, respectively. The transverse dimensions of the silicon channel are varied from 8×8 nm^2 to 3×3 nm^2. For all the device cross sections considered, the width of the oxide on both sides of the channel is 200 nm, the channel is doped to 3×10^{15} cm^{-3}, and the channel is assumed to be homogeneous and infinitely long. For the SiNWs considered, the confinement is along the y and z directions and the electrons are allowed to move freely in the x direction.

2.2 Self-consistent 2D Poisson–2D Schrödinger solver

The Hamiltonian for an electron, residing in one of the six valleys (ν) is of the form

$$H_0(\mathbf{r}) = -\left(\frac{\hbar^2}{2m_x^\nu}\frac{\partial^2}{\partial x^2} + \frac{\hbar^2}{2m_y^\nu}\frac{\partial^2}{\partial y^2} + \frac{\hbar^2}{2m_z^\nu}\frac{\partial^2}{\partial z^2}\right) + V(y,z) = H_{0\parallel}(x) + H_{0\perp}(y,z), \tag{1}$$

where $\mathbf{r} = (x, y, z)$, $V(y, z)$ is the potential energy profile of the confining potential in the (y, z)-plane (obtained from the Hartree potential, the solution to the 2D Poisson's equation), $H_{0\parallel}$ is the parallel part of H_0 (associated with the motion along the axis of the wire), and the transverse part is defined as

$$H_{0\perp}(y,z) = -\frac{\hbar^2}{2m_y^\nu}\frac{\partial^2}{\partial y^2} - \frac{\hbar^2}{2m_z^\nu}\frac{\partial^2}{\partial z^2} + V(y,z). \tag{2}$$

The basis-states of the unperturbed Hamiltonian are assumed to be of the form

$$\psi_{\nu,n}(\mathbf{r}) = \frac{1}{\sqrt{L}}e^{ik_x x}\psi_{\nu,n}(y,z), \tag{3}$$

where k_x is the wavevector along the axis of the wire of length L and the wavefunction $\psi_{\nu,n}(y, z)$ of subband with energy $\mathcal{E}_{\nu,n}$ satisfies the 2D Schrödinger equation

$$H_{0\perp}(y,z)\psi_{\nu,n}(y,z) = \mathcal{E}_{\nu,n}\psi_{\nu,n}(y,z). \tag{4}$$

Because of the pronounced mass anisotropy in the Si material system and the multi-valley nature of the lowest conduction bands, the six conduction band valleys are included through a standard three-valley-pair model. Valley pair 1 along the (100) direction have masses $m_x = m_l$ and $m_y = m_z = m_t$, valley pair 2 along the (010) direction have masses $m_x = m_z = m_t$ and $m_y = m_l$, and valley pair 3 along the (001) direction have masses $m_x = m_y = m_t$ and $m_z = m_l$.

An accurate description of the charge and potential in a nanowire requires a self-consistent solution of the 2D Schrödinger equation (4) and the 2D Poisson equation

$$\frac{\partial}{\partial y}\left[\epsilon(y,z)\frac{\partial\varphi(y,z)}{\partial y}\right] + \frac{\partial}{\partial z}\left[\epsilon(y,z)\frac{\partial\varphi(y,z)}{\partial z}\right] = -e\left[N_D^+ - N_A^- + p(y,z) - n(y,z)\right], \tag{5}$$

where $\varphi(y, z)$ is the electrostatic Hartree potential and $V(y, z) = -e\varphi(y, z)$, $\epsilon(y, z)$ is the spatially-dependent dielectric constant, N_D^+ and N_A^- are the ionized donor and acceptor concentrations, and $n(y, z)$ and $p(y, z)$ are the electron and hole densities, respectively. The electron density is calculated using

$$n(y,z) = 2\sum_{\nu,n} N_{\nu,n}\left|\psi_{\nu,j}(y,z)\right|^2, \tag{6}$$

where the factor 2 accounts for the valley degeneracy and $N_{\nu,n}$ is the electron line density in the n-th subband of the ν-th valley pair, given by

$$N_{\nu,n} = \frac{1}{\pi\hbar}\sqrt{2m_x^\nu k_B T}\,\mathcal{F}_{-1/2}\left(\frac{E_F - E_{\nu,n}}{k_B T}\right), \tag{7}$$

where E_F is the Fermi energy, k_B is the Boltzmann constant, and T is the temperature. The Fermi-Dirac integral of order

$-1/2$ can be approximated as [21, 22]

$$\mathcal{F}_{-1/2}(\eta) = \int_0^\infty \frac{u^{-1/2}du}{1+e^{u-\eta}} \simeq \frac{\sqrt{\pi}}{e^{-\eta} + \sqrt{\frac{\pi}{2}} \frac{1}{\sqrt{\eta+b+[a+(|\eta-b|)^c]^{1/c}}}}, \quad (8)$$

where $\eta = (E_F - E_{v,n})/k_BT$, $a = 6.68$, $b = 1.72$, and $c = 4.11$. These equations can be solved by using finite difference discretization scheme described in [23]. The steps involved in solving these two equations self-consistently is described below.

Step 1 Initialization: Poisson's equation is solved in the entire 2D cross-section, whereas the Schrödinger equation needs to be solved only in the silicon region and a small region of oxide near the Si-SiO_2 interface. As most of the interesting physics happens near the interfaces, a fine mesh is used near the Si interface with oxide and metal. Away from the interfaces, a coarse mesh is used. The use of a non-uniform mesh reduces the size of the matrices to be solved.

Step 2 Boundary Condition: A Dirichlet boundary condition is employed to model the ohmic contacts, therefore the potential at the contacts is obtained by summing the externally applied gate bias (V_g) and the potential obtained by imposing the charge neutrality condition (by setting the left hand side of Poisson's equation to zero) (Fig. 1, top left panel). Continuity of the electric displacement field at the interface of silicon and oxide is used to determine the initial potential in the oxide. As the oxide at the sides of the silicon channel are thick, the field in the oxide goes to zero at the surface of oxide (see Fig. 1 top right panel).

Step 3: Calculate the coefficients of discretized Poisson and Schrödinger equations.

Step 4: Solve the Poisson equation.

Step 5: Update the central coefficient of Schrödinger equation using the potential from the Poisson Solver.

Step 6: Solve the Schrödinger equation.

Step 7: Calculate the quantum corrected electron density using the wavefunctions and energy levels obtained from the Schrödinger solver (use (6)).

Step 8: Update the coefficients of Poisson equation that depend on the electron density.

Step 9: Solve Poisson's equation.

Step 10: Check if the new potential obtained from the Poisson solver has converged (typical convergence criterion is max(old potential–new potential) $< 10^{-5}$ V). If the potential has converged go to Step 11, if not repeat from Step 5.

Step 11: Once the potential converges, the following profiles from the Poisson-Schrödinger solver are exported into the Monte Carlo solver. (a) The potential profile (used in the calculation of SRS). (b) The energy level and wave

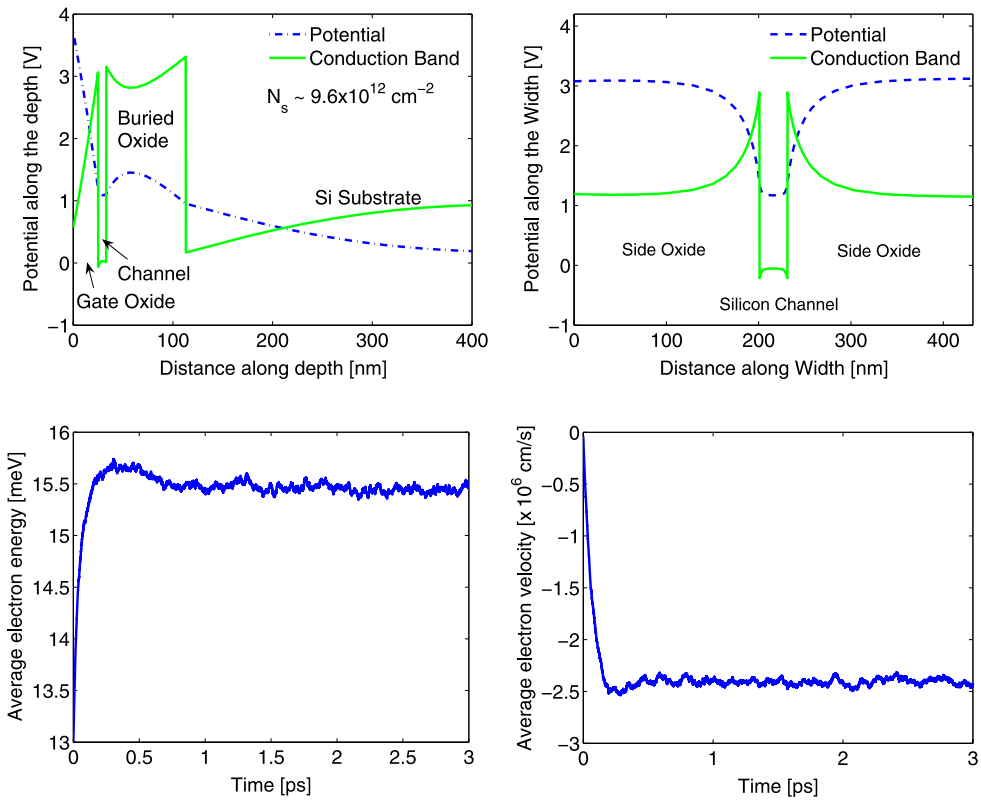

Fig. 1 Results from the Poisson-Schrödinger-Monte Carlo solver. *Top panels*: The potential profile along the y direction (*top left*) and the z direction (*top right*) obtained from the self-consistent Poisson-Schrödinger solver. *Bottom panels*: Variation of the electron energy (*left*) and velocity (*right*) with time from the EMC. Steady state (indicated by the saturation of energy and velocity) is reached on picosecond timescales

function of each subband in all three valley pairs (used in the calculation of all scattering rates). (c) Line density in each subband (used in MC to initialize electrons in different subbands). (d) Electron sheet density (used to calculate the effective field from the gate). (e) Mesh spacing profile. Sample potential profile across the wire, obtained from the Poisson-Schrödinger solver, is presented in the top two panels of Fig. 1.

2.3 Ensemble Monte Carlo solver

The ensemble Monte Carlo (EMC) technique is an well-established, efficient, stochastic technique for the simulation of non-equilibrium transport in semiconductor materials and devices [2, 24]. During the simulation, one tracks the motion of an ensemble of particles. The free flight of a particle under external fields gets terminated by instantaneous random scattering events. Relevant scattering mechanisms in silicon are acoustic phonon scattering, intervalley scattering (mediated by large momentum acoustic and optical phonons), ionized impurity scattering, and surface roughness scattering [16, 23]. The EMC algorithm consists of generating random free flight times for each particle, choosing the type of scattering occurring at the end of the free flight, changing the final energy and momentum of the particle after scattering and then repeating the procedure for the next free flight. Sampling the particle motion at various times throughout the simulation allows for a statistical estimation of the physically interesting quantities such as the single-particle distribution function, the average drift velocity in the presence of an applied electric field, the average energy of the particles, etc. Monte Carlo accounts for repopulation of subbands due to scattering in addition to calculating lateral carrier motion.

The ensemble Monte Carlo transport kernel is used to simulate the electron transport along the axis of the wire under the influence of the confining potential in the transverse directions and a very small lateral electric field along the channel. The long wire approximation implies that the transport is diffusive (the length exceeds the carrier mean free path) and therefore justifies the use of the Monte Carlo method [2, 24] to simulate electron transport. Electrons are initialized such that their average kinetic energy is $(1/2)k_BT$ (thermal energy for 1D) and are distributed among different subbands in accordance with the equilibrium distribution of the states obtained from the Poisson-Schrödinger solver. Since the electrons are confined in two transverse directions, they are only scattered in either the forward or the backward direction; consequently, just the carrier momentum along the length of the wire needs to be updated after each scattering event. Upon reaching steady-state (indicated by saturation of the average electron energy and drift velocity, see bottom panel of Fig. 1), mobility is calculated from the ensemble average of the electron velocities [2].

3 Electron mobility variation with the SiNW cross section

The variation of the electron mobility when the SiNW cross section is decreased from 8×8 nm^2 to 3×3 nm^2 is shown in Fig. 2. The three curves correspond to three different transverse effective fields. Irrespective of the effective field from the gate, the mobility decreases with increasing spatial confinement mainly due to the monotonic increase in the confinement-induced part of surface roughness scattering (SRS) and the intrasubband phonon scattering. At low and moderate effective fields from the gate, the mobility is determined by the scattering from phonons and the confinement-induced part of the SRS, whereas at high fields mobility is limited by the SRS (all three terms in the SRS overlap integral [16] play crucial roles).

At high fields from the gate, when the wire cross section is reduced from 8×8 nm^2 to 5×5 nm^2, the first term in the SRS overlap integral increases, whereas the second and the third terms decrease due to the onset of volume inversion. Consequently, the mobility shows a very small change for these cross sections. But, when the wire cross section is smaller than 5×5 nm^2, all the terms in the SRS overlap integral increase with decreasing wire cross section and result in a monotonic decrease in mobility with increasing spatial confinement.

At low and moderate fields from the gate, with decreasing wire cross section: the intrasubband phonon scattering increases due to the increase in the electron-phonon overlap integral [16]; intersubband scattering and intervalley phonon scattering decreases due to subband modulation; SRS increases due to the increase in the first term in the SRS overlap integral with increasing confinement. Overall the mobility decreases with decreasing wire cross section. It should be noted that, at low transverse fields, the mobility variation for wires of cross section larger than 7×7 nm^2 becomes

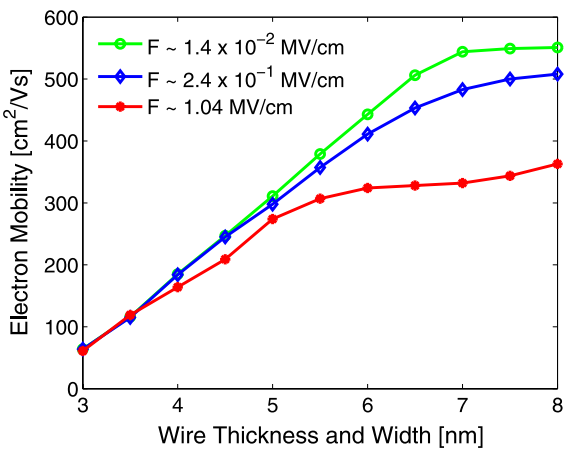

Fig. 2 Variation of the electron mobility with the SiNW cross section at three different transverse fields (reprinted with permission from [16])

very small. This is because of the interplay between a simultaneous increase in intersubband scattering (number of occupied subbands increases) and a decrease in intrasubband scattering (electron-phonon overlap integral decreases) with increasing wire cross section. A similar weak dependence of the electron mobility in cylindrical SiNWs with diameters greater than 6 nm has also been reported by Jin et al. [14].

4 Conclusion

A self-consistent Poisson-Schrödinger-Monte Carlo solver has been developed to study the effect of 2D spatial confinement on the mobility of electrons in SiNWs. Electron mobility is found to decrease with decreasing wire cross section predominantly because of the strong increase in surface roughness scattering. In contrast to bulk MOSFETs, in which the SRS plays an important role only for high fields from the gate, electrons in very thin SiNWs are strongly influenced by the roughness regardless of the transverse field.

Acknowledgements This work was supported by the NSF through the University of Wisconsin MRSEC (DMR-0520527) and by the AFOSR YIP program (FA9550-09-1-0230).

References

1. Sakaki, H.: Jpn. J. Appl. Phys. **19**(12), L735 (1980)
2. Jacoboni, C., Reggiani, L.: Rev. Mod. Phys. **55**, 645 (1983)
3. Ramayya, E.B., Vasileska, D., Goodnick, S.M., Knezevic, I.: IEEE Trans. Nanotechnol. **6**(1), 113 (2007)
4. Wang, J., Polizzi, E., Ghosh, A., Datta, S., Lundstrom, M.: Appl. Phys. Lett. **87**, 043101 (2005)
5. Zheng, Y., Rivas, C., Lake, R., Alam, K., Boykin, T.B., Klimeck, G.: IEEE Trans. Electron Devices **52**(6), 1097 (2005)
6. Luisier, M., Schenk, A., Fichtner, W., Klimeck, G.: Phys. Rev. B **74**, 205323 (2006)
7. Luisier, M., Schenk, A., Fichtner, W.: Appl. Phys. Lett. **90**, 102103 (2007)
8. Buin, A.K., Verma, A., Svizhenko, A., Anantram, M.P.: Nano Lett. **8**(2), 760 (2008)
9. Rurali, R.: Rev. Mod. Phys. **82**, 427 (2010)
10. Cui, Y., Zhong, Z., Wang, D., Wang, W.U., Lieber, C.: Nano Lett. **3**(2), 149 (2003)
11. Koo, S.M., Fujiwara, A., Han, J.P., Vogel, E.M., Richter, C.A., Bonevich, J.E.: Nano Lett. **4**(11), 2197 (2004)
12. Sharma, A.K., Zaidi, S.H., Lucero, S., Brueck, S.R.J., Islam, N.E.: IEE Proc. Circuits Devices Syst. **5**(151), 422 (2004)
13. Kotlyar, R., Obradovic, B., Matagne, P., Stettler, M., Giles, M.D.: Appl. Phys. Lett. **84**(25), 5270 (2004)
14. Jin, S., Fischetti, M.V., Tang, T.: J. Appl. Phys. **102**(8), 083715 (2007)
15. Godoy, A., Ruiz, F., Sampedro, C., Gámiz, F., Ravaioli, U.: Solid-State Electron. **51**, 1211 (2007)
16. Ramayya, E.B., Vasileska, D., Goodnick, S.M., Knezevic, I.: J. Appl. Phys. **104**(6), 063711 (2008)
17. Lenzi, M., Palestri, P., Gnani, E., Reggiani, S., Gnudi, A., Esseni, D., Selmi, L., Baccarani, G.: IEEE Trans. Electron Devices **55**(8), 2086 (2008)
18. Gunawan, O., Sekaric, L., Majumdar, A., Rooks, M., Appenzeller, J., Sleight, J.W., Guha, S., Haensch, W.: Nano Lett. **8**, 1566 (2008)
19. http://www.caam.rice.edu/software/ARPACK/
20. Majima, H., Ishikuro, H., Hiramoto, T.: IEEE Electron Device Lett. **21**(8), 396 (2000)
21. Aymerich-Humet, X., Serra-Mestres, F., Millan, J.: Solid-State Electron. **24**, 981 (1981)
22. Abramo, A., Cardin, A., Selmi, L., Sangiorgi, E.: IEEE Trans. Electron Devices **47**, 1858 (2000)
23. Knezevic, I., Ramayya, E.B., Vasileska, D., Goodnick, S.M.: J. Comput. Theor. Nanosci. **6**, 1725 (2009)
24. Fischetti, M.V., Laux, S.E.: Phys. Rev. B **48**(4), 2244 (1993)